Mechanical Design Calculations of Flywheel Generator

Md Zafar Anwar , **Nilanjan Sen, Jitendra Prasad Khatait, and Sudipto Mukherjee**

Abstract Flywheels generator is suited where a pulsed current generation is required. It has a higher energy density as compared to capacitor banks. This paper focuses on design calculations related to flywheel energy storage system (FESS) being developed at IIT Delhi. The flywheel rotor, filament wound carbon fibre/epoxy composite, will have storage capacity 10 MJ of energy at 17,000 rpm with energy storage density of 77.5 J/g and power density of 1.94 kW/g. At such a high speed, issues related to air drag, inertial forces on a rotor, dynamic forces on bearings, and vibration become critical. In this paper, we analysed these issues and proposed appropriate solutions.

1 Introduction

Pulsed current has applications like electromagnetic propulsion, where the release of energy takes place in milliseconds. This pulsed current can be achieved through capacitor banks or flywheel generators. Flywheel generator has a higher energy density compared to conventional capacitor banks. Flywheel energy storage system (FESS), with a capacity of 10 MJ at 17,000 rpm with a 10% discharge rate per cycle, is to be constructed at IIT Delhi. The planned setup will have an energy storage density of 77.5 J/g and a power density of 1.94 kW/g. This energy density is much higher than that of capacitor bank 1 J/cc [1]. In this paper, we discussed the mechanical design calculations for FESS. Issues like stresses and air drag loss (windage loss) have been analysed.

Md Z. Anwar (✉) · N. Sen · J. P. Khatait · S. Mukherjee
Indian Institute of Technology Delhi, New Delhi 110016, India

J. P. Khatait
e-mail: jpkhatait@mech.iitd.ac.in

S. Mukherjee
e-mail: sudipto@mech.iitd.ac.in

Fig. 1 Design schematic of
the flywheel rotor assembly
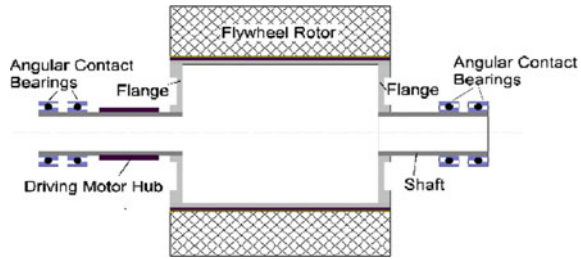
In Sect. 2, we discussed the design schematic of the setup. Next, design calcula-
tion is presented along with the modelling of various components. In this section,
we started with a consideration of NdFeB magnets followed by the calculation for
interference amongst the rotor layers. Then, we proceed with stress analysis of rotor
and calculation of static and dynamic deflections of the assembly. We discussed the
effect of anisotropic degree on hoop stress and deflection. Further, we presented a
modified version of Rayleigh's method to calculate the critical speed of complete
assembly. At last, losses due to air drag and the effect of evacuation are discussed.

2   Design Schematic

The flywheel generator uses a spindle motor of 175 kW to drive the rotor. The
motor torque is transmitted to the rotor through a hub mounted over a steel shaft.
The rotor consists of aluminium layer for shielding, Neodymium magnets (NdFeB)
permanent magnets for the magnetic field, titanium sleeve for pre-compression of
magnets, and filament wound carbon fibre-epoxy composite rotor for providing the
inertia. High-speed ceramic angular contact bearings support this rotor assembly
via flexible flanges. These angular contact bearing are pre-compressed to increase
the stiffness of bearing. This whole assembly is mounted over a stator consisting of
winding for generating the electric pulse. The design schematic is shown in Fig. 1.
The entire setup is then packed into an evacuated chamber.

3   Modelling and Design Calculation

3.1   NdFeB Magnet and Equivalent Layer

For applying a magnetic field, Neodymium Iron Boron (NdFeB) magnets are used due
to high magnetic strength. NdFeB magnets have a low tensile strength of ~80 MPa,
limiting the operational speed; therefore, it is compressed using titanium sleeve to
~600 MPa (compressive strength ~850 MPa) such that upon rotation, compressive

Table 1 Conditions and calculated value of interference between layers

Condition		Computed Value	
$(\sigma_{Eq})_c$	−600 Mpa	$(\delta_i)_{Eq-Ti}$	0.98 mm
$(\delta_i)_{Al-Eq}$	0	$(\sigma_{Al})_c$	-302 Mpa
$(\delta_i)_{Ti-CF}$	0	$(\sigma_{Ti})_c$	163 Mpa
		$(\sigma_{CF})_c$	70 Mpa

stress is relieved allowing to achieve speed higher than 17,000 rpm. Magnets, along with non-magnetic filler material (aluminium), form a cylindrical layer whose equivalent modulus is given by Eq. (1). This equivalent modulus is used to calculate the required interference fit between magnets and titanium sleeve.

$$\frac{1}{E_{eq}} = \frac{\chi_{pm}}{E_{pm}} + \frac{(1 - \chi_{pm})}{E_{Al}} \tag{1}$$

where E_{eq} is the modulus of the equivalent layer, χ_{pm} is length fraction of NdFeB in the layer, E_{pm} is the modulus of PM, E_{Al} is the modulus of aluminium.

Interference Calculation. To compress the magnets, interference is calculated using thin cylinder approximation. Interference amongst the segments not only keeps the magnet layer in compression but also reduces the radial stress among other segments (Table 1).

3.2 Stress Analysis of Rotor

At high speed, stresses become critical in rotors. There are four cylindrical layers in the flywheel rotor (as discussed before) with different interference fits. The strength and radial region of each segment are given in Table 2. The hoops stress, radial stress, and radial deflection are calculated using equations for rotating anisotropic disc along with boundary conditions [2–4]. The results are shown in Fig. 2.

The PM layer is pre-compressed to ~600 MPa, which is relieved to ~200 MPa (compressive) at 17,000 rpm. The maximum circumferential stress in the system is

Table 2 Radial region and strength of individual layers of the flywheel rotor

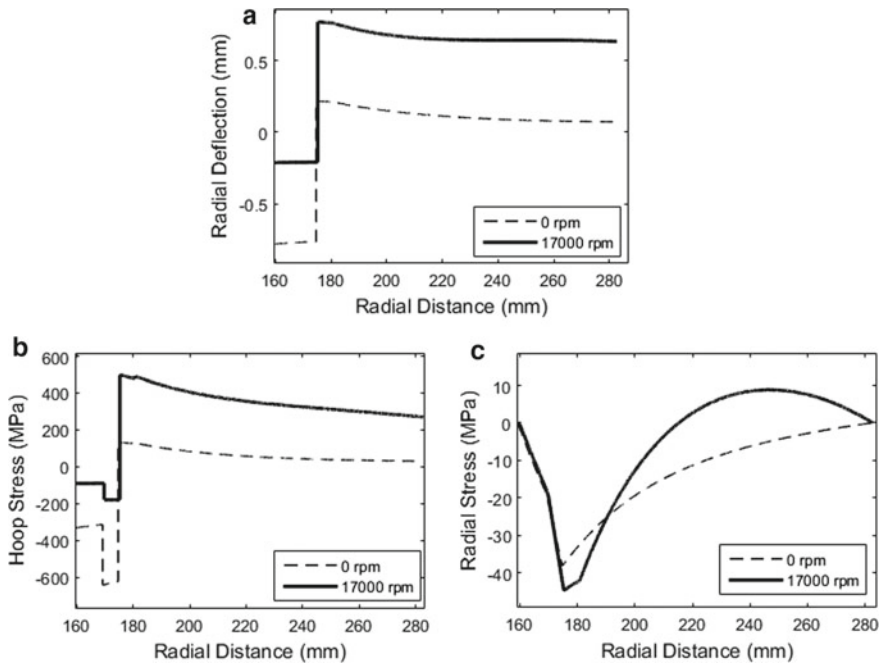|	Radial stretch	Strength (Mpa)
Aluminium alloy shield	160–170 mm	~500 (compressive)
NdFeB magnets	170–175 mm	~850 (compressive)
Titanium sleeve	175–180 mm	~800 (tensile)
Carbon fibre-Epoxy composite	180–282 mm	~1200 (hoops); ~90 (Radial)

Fig. 2 **a** Radial deflection, **b** hoop stress, and **c** radial stress distribution

~500 MPa (tensile) in the titanium sleeve and composite rotor. The stresses in all layers are found to be within their respective allowable limits.

3.3 Max Deflection of System

The rotor assembly consists of five horizontal sections with different section properties. These sections are modelled as connected beams, and loading conditions are applied with boundary conditions to compute the deflection (say y). The assembly bends due to gravitational force (say G) and centrifugal force (say $C(y)$). Gravitational force is independent of deflection, while the centrifugal force is a function of deflection (y) and changes direction during rotation. These two forces are balanced by the restoring force (say K) of the rotor, which also depends on the deflected value.

Maximum deflection occurs when centrifugal force aligns with the gravitational force. The deflection is calculated using an iterative method, and the solution converges to give the result. However, near critical speed, the solution does not converge. This is consistent with the theory that near critical speed the deflection value tends to infinity.

$$K(y_i) = G + C(y_{i-1}) \tag{2}$$

Fig. 3 Static deflection and max deflection at 17,000 rpm in the assembly
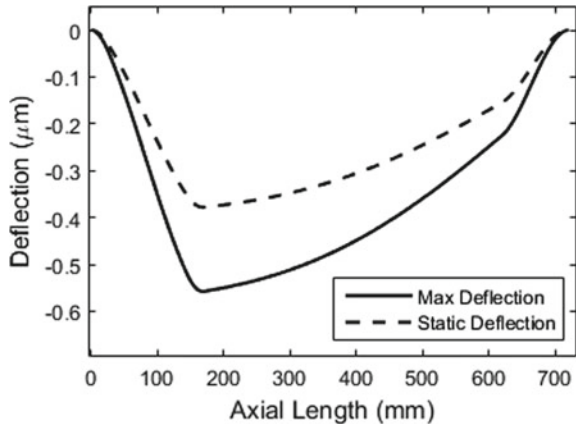
In the calculation, it is assumed that the rotor has an eccentricity of 1 μm (as per the facility available for balancing the rotor). Figure 3 shows the static deflection (due to gravitational force) and maximum possible deflection (due to centrifugal force and gravitational force combined).

3.4 Anisotropic and Isotropic Properties

Apart from high strength-to-weight ratio, composite rotors have its advantage due to variation in the anisotropic degree $\left(\lambda = \sqrt{E_\theta/E_r}\right)$. Isotropic rotors have a significant variation in hoop stress across the section, maximum at the inner wall and minimum at the outer surface. This results in an unoptimised utilisation of material strength. Anisotropic rotors can be designed such that there is uniform stress across the section. This not only reduced the value of maximum hoop stress but also maintained uniform stress throughout the radial span (Fig. 4).
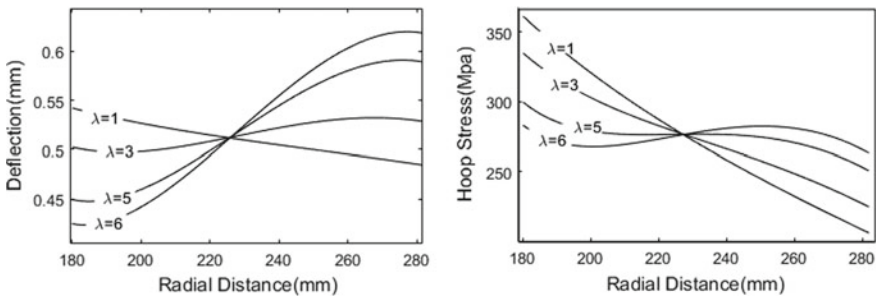

Fig. 4 Trend of deflection and hoop stress with changing anisotropic degree (λ)
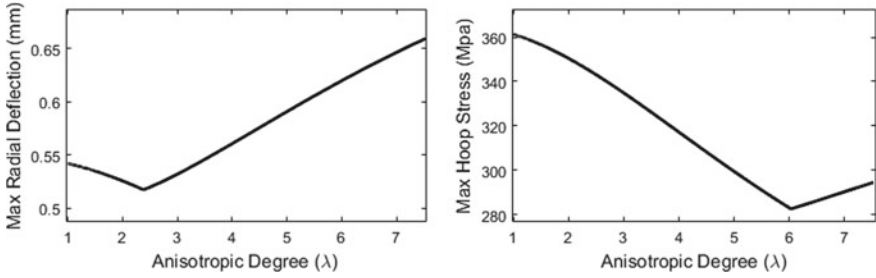
Fig. 5 Effect of anisotropic degree on max deflection and max hoop stress in a rotating disc

The anisotropic degree can be varied to achieve the optimised value. At 17,000 rpm and $E_\theta = 120$ Gpa, for minimum hoop stress optimised value, is $\lambda = 6$, while for minimum deflection is $\lambda = 2.5$ as shown in Fig. 5. Depending upon the design requirement, the anisotropic properties are designed to achieve the optimised result. The carbon-epoxy filament wound rotor in the flywheel has a value of $\lambda = 3.65$.

The value of anisotropic degree λ can be optimised by selecting modulus of the fibre and epoxy and by varying volume fraction of the fibre and matrix [3].

$$E_\theta = E_f V_f + E_m V_m \tag{3}$$

$$E_r = \frac{E_f E_m}{V_m E_f + V_f E_m} \tag{4}$$

where E_f, E_m are elastic moduli of fibre and matrix, respectively; V_f, V_m are volume fraction of fibre and matrix.

3.5 Critical Speed of the System

The critical speed of the assembly, consisting of five sections having different properties, is calculated using a similar approach as of Rayleigh's method, but instead of assuming a shape function, here actual deflection curve is used. Rayleigh's method considers deflection as per the shape function without considering the differences in stiffness [5]. This results in inaccurate potential and kinetic energy of each section.

$$\omega^2 = \frac{\int_0^{l_1} E_1 I_1 \left(\frac{\mathrm{d}^2 W(x)}{\mathrm{d}x^2}\right)^2 \mathrm{d}x + \int_{l_1}^{l_2} E_2 I_2 \left(\frac{\mathrm{d}^2 W(x)}{\mathrm{d}x^2}\right)^2 \mathrm{d}x + \cdots}{\int_0^{l_1} \rho_1 A_1 (W(x))^2 \mathrm{d}x + \int_{l_1}^{l_2} \rho_2 A_2 (W(x))^2 \mathrm{d}x + \cdots} \tag{5}$$

where ω is critical angular velocity, E is Young's modulus of material, I is section modulus, ρA is mass per unit length, $W(x)$ is the actual static deflection curve.

The Rayleigh method with assumed shape function gives a critical speed of 122.7 krpm, while the above approach gives 54 krpm. In Rayleigh's method with assumed shape function the flywheel section stores 96% of total PE, but in the real case, this section is rigid and has negligible deformation as compared to other parts, and hence, PE which is due to strain is just 6% of the total. This is the reason that Rayleigh's method gives the inaccurate results, where the section properties vary drastically.

3.6 Windage Losses

Air drag on rotor surfaces causes significant power loss. At atmospheric pressure, the power loss is ~200 kW. Power loss at surfaces depends on fluid properties and rotor dimensions (Eq. 6) [6, 7]. The density of air depends on pressure; hence, evacuating the chamber reduces the power loss. Power loss reduces to ~50 kW at 10 kPa (Fig. 6).

$$P_w = \pi C_d \rho r^4 \omega^3 L \tag{6}$$

$$\sqrt{C_d} \left\{ 2.04 + 1.768 \ln \left(\text{Re} \sqrt{C_d} \right) \right\} - 1 = 0 \tag{7}$$

where P_w is power loss or windage loss (W), ρ is the density of the fluid (kg/m^3), r is the radius of cylinder (m), ω is angular velocity(rad/sec), C_d is skin friction coefficient, L is the length of the rotor, Re is Reynold's number.

.

Fig. 6 Windage losses as a function of pressure
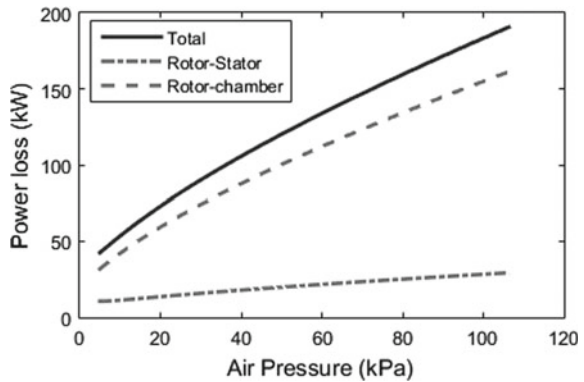
4 Conclusion

In this paper, design calculation of the main parameters of the flywheel assembly has been discussed. The design was done based on energy storage capacity of 10 MJ at 17,000 rpm. The hoops and radial stresses in the flywheel rotor are investigated along with the modelling of the NdFeB magnet layer and filler material as an equivalent layer. Benefits of anisotropic material over isotropic were analysed. The deflection in the rotor assembly has been calculated using an iterative method, which was further used in finding critical speed. The critical speed of the assembly was determined with a modified version of Raleigh's method and found out that assuming shape function can result in a significant deviation from actual critical speed. Air drag, which is the primary cause of the power loss in a high-speed flywheel, has been discussed and shown that evacuating the chamber results in a significant reduction of power loss.

Overall through this paper, general design parameter has been discussed. However, detailed simulation results need to be considered in the next step to build the prototype. Further work is to be done to improve the energy storage capacity and achieve higher operating speed.

References

1. Curtiss DH, Mongeau PP, Puterbaugh RL (1995) Advanced Composite flywheel structural design for a pulsed disk alternator. IEEE Trans Magn 31(1):26–31
2. Vrancik JE (1968) Prediction of windage power loss in alternators. National Aeronautics and Space Administration, Washington, D. C.
3. Zhang Q, Wu S, Yu C, Cui S, Song L (2011) Design of a Model-scale air-core compulsator. IEEE Trans Plasma Sci 39(1):346–353
4. Zhang F, Du G, Wang T, Liu G, Cao W (2015) Rotor retaining sleeve design for a 1.12-MW high-speed PM machine. IEEE Trans Ind Appl 51(5):3675–3685
5. Maslen EH, Schweitzer G (2009) Aerodynamic losses, windage losses. In: Magnetic bearings. Springer, Berlin, pp 141–145
6. Rao SS (2004) Rayleigh s method. In: Mechanical vibrations. Prentice Hall, Upper Saddle River, pp 742–745
7. Pradeep Kumar V, Swarup S, Rajput S, Kumar G, Nomula AP, Jadhav KB, Taral SY, Daniel KJ, Datar S (2019) Design and development of 4-MJ capacitor bank-based pulsed power system for electromagnetic launcher. IEEE Trans Plasma Sci 1–9